scientific reports

Check for updates

OPEN

Physiological and morphological effects of a marine heatwave on the seagrass *Cymodocea nodosa*

Alizé Deguette[1], Isabel Barrote[1,2,3] & João Silva[1,3]✉

Marine heatwaves (MHWs) are increasing in frequency and intensity as part of climate change, yet their impact on seagrass is poorly known. The present work evaluated the physiological and morphological responses of *Cymodocea nodosa* to a MHW. *C. nodosa* shoots were transplanted into a mesocosm facility. To simulate a MHW, water temperature was raised from 20 to 28 °C, kept 7 days at 28 °C, cooled down back to 20 °C and then maintained at 20 °C during an 8-day recovery period. The potentially stressful effects of the simulated heatwave on the photosynthetic performance, antioxidative-stress level and area *vs* dry weight ratio of leaves were investigated. The maximum quantum yield of photosystem II (ΦPSII) increased during the heatwave, allowing the plants to maintain their photosynthetic activity at control level. Negative effects on the photosynthetic performance and leaf biomass of *C. nodosa* were observed during the recovery period. No significant oxidative stress was observed throughout the experiment. Overall, although *C. nodosa* showed a relative tolerance to MHWs compared to other species, its population in Ria Formosa is likely to be negatively affected by the forecasted climate change scenarios.

Heatwaves are often pointed out as yet another negative consequence of climate change and global warming. Only recently, and pressured by the urgency of the climatic threat, the scientific community started qualifying and understanding the marine heatwave (MHW) phenomenon. The Intergovernmental Panel on Climate Change (IPCC) defined MHW as "an event at a particular place and time of the year that is rare and predominately, but not exclusively, defined by a relative threshold; that is, an event rarer than 90th or 99th percentile of a probability density function", in the Special Report on the Ocean and Cryosphere (SROC)[1]. MHW occur at any time of the year, everywhere in the world, for a period ranging from a few days to several weeks at varying intensities. Their frequency and intensity have severely increased in the past century[2], causing massive extinctions events (e.g. "The Blob", a large mass of high-temperature water in the Pacific Ocean that killed nearly a million seabirds in Alaska and California in 2015–2016)[3], range shifts[4] and coral bleaching (mass coral mortality occurred in the Great Barrier Reef in 2016, with losses exceeding 50%)[5–8].

Seagrasses are angiosperms (flowering plants) adapted to marine life, accounting for about 60 species worldwide[9]. These clonal plants, which shoots grow from the expansion of rhizomes[10] and are found worldwide along tropical, temperate, and boreal latitudes, except in the Antarctic region, colonising intertidal areas and shallow waters in subtidal zones[11]. Seagrass meadows are among the most ecologically valuable estuarine and coastal ecosystems, providing a large range of essential ecosystem services. They offer valuable feeding, spawning and nursery grounds for numerous species of flora and fauna[12] and enhance the production and biodiversity of adjacent ecosystems[13]. Seagrass beds slow down the currents, trap suspended particles and, in this way, increase light penetration[14]. They have been increasingly studied because of their nitrogen fixation capacity[15], their role as carbon sinks[16–19], and their major importance in "blue carbon" sequestration and export[20]. Although they represent less than 0.1% of the ocean surface, seagrasses are responsible for 20% of oceanic carbon sequestration globally[21,22]. Regrettably, seagrass meadows are declining globally at a dramatic rate (110 km^2 $year^{-1}$ since 1980 i.e., 5% $year^{-1}$ globally or at least 1/3 since World-War II)[23,24] because of the environmental changes they face. Notably, MHWs have been proved to be one of the major drivers of seagrass decline (36% of Shark Bay's—Western Australia—seagrass meadows were negatively affected by a MHW in 2010/11)[25]. In fact, a temperature increase above the optimum temperature of seagrasses reduces the photosynthetic rate and leave's productivity and increases respiration, photosynthetic stress responses and biomass losses[26,27]. In addition, these effects are even more considerable as the number of thermal stress days increases, with species-specific responses[27,28].

[1]Centre of Marine Sciences, University of Algarve, Campus of Gambelas, 8005-139 Faro, Portugal. [2]Faculty of Science and Technology, University of Algarve, Campus of Gambelas, 8005-139 Faro, Portugal. [3]These authors contributed equally: Isabel Barrote and João Silva. ✉email: jmsilva@ualg.pt

Previous studies showed that heat stress negatively impacts the metabolism of *Zostera noltii*[29] and *Zostera marina*[30,31], lowering the flowering and reproductive intensity of this species[32] and leading to important shifts in physiological stress indicators (inhibition of photosynthetic efficiency (-23.9%), increased respiration (+ 58.3%) and decreased carbohydrate decomposition products)[33]. A study showed that the species *Cymodocea nodosa* and *Posidonia oceanica* were able to recover from a simulated MHW, with shifts in carbon allocation strategies that differ between shoots coming from different thermal environments (thermal adaptation)[34]. *C. nodosa* showed the ability to change its metabolism to handle short thermal stress (shifts in photosynthetic pigments concentration, increased antioxidant activity and CO_2 assimilation)[35].

In Europe, 35 684 ha of seagrass meadows disappeared between 1869 and 2016, i.e., 29% of the documented area[36]. The same study showed that the highest proportions of declines were reported for the species *Z. marina* and *C. nodosa* (net losses of 57% and 46% of the documented area, respectively). Despite the general decline of seagrasses in Europe between 1869 and 2016, gain was reported in the 2000s, for the first time since the 1950s (20% net gain in area per decade in the 2000s)[36], showing a significant trend reversal as a result of conservation and restoration actions. Thus, seagrass decline is neither irreversible nor to be generalised: hope remains to maintain or even improve the services they provide.

C. nodosa (Ucria) is the most abundant subtidal seagrass species in Ria Formosa coastal lagoon, Southern Portugal, where it covered an area of 0.913 km^2 in 2007[37]. It is a temperate-warm adapted species, resistant to relatively high-water temperatures (25–32 °C)[38,39]. Its distribution ranges from its northern limit on the southern Portuguese coast to its southern limit in Senegal[40]. As a tropical-originated species, *C. nodosa* has a high optimum temperature range (24.5 and 31.0 ± 0.5 °C for growth and photosynthesis, respectively) when compared to temperate species in the Mediterranean, such as *Z. marina* (15.3 ± 1.6 and 23.3 ± 1.8 °C, respectively)[41]. While the effects of MHWs and heat shocks have been studied mainly on *Z. marina*[31,33,42,43], they have been poorly studied for *C. nodosa*. Based on the existing literature, we hypothesize that negative effects of MHWs are also to be expected on this species (e.g., lower productivity/photosynthetic activity, increased oxidative damage), despite its potential ability to thrive in warm waters.

The objective of this work was to investigate the morphological changes and physiological capacity of *C. nodosa* to cope with MHWs in Ria Formosa, in the framework of evaluating and forecasting the species tolerance under climate change scenarios that include more frequent and intense MHWs. Specifically, we investigated the plant's physiological and morphological response throughout the peak of a MHW and the existence of putative sequels, evaluated during a recovery period. The absolute temperature value used for the MHW simulation was based on in situ temperature records and the definition and classification of MHWs. The photosynthetic performance of different tissue ages, the antioxidant activity, the potential oxidative damage and changes in leaf biomass were assessed.

Results

Photosynthetic activity. *Photosynthesis-Irradiance (P-I) curves.* *C. nodosa* leaves' photosynthetic activity responded to light stimulation by a typical Photosynthesis-Irradiance (P-I) hyperbolic-shaped response with increasing light intensity (Fig. 1).

The photosynthetic parameters α, P_m and I_k were significantly lower in leaves from plants recovering from the heatwave than control ($p < 0.001$, $p < 0.001$ and $p = 0.008$, respectively; Table 1).

While α was *ca*. twofold lower than control, P_m was *ca*. fourfold times lower and therefore, I_k decreased significantly. Conversely, no significant difference was observed in leaves sampled during the heatwave.

Chlorophyll fluorescence imaging (CFI). The Chlorophyll Fluorescence Imaging (CFI) pictures allow to measure, visualize and pinpoint potential differences in the effective quantum yield of electron transport through photosystem II (Φ_{PSII}), along the leaves' surface and between different tissue ages (Fig. 2).

During the heatwave, Φ_{PSII} was significantly higher in heatwave (HW) leaves than control (C) ($p = 0.008$) and old leaf tissues displayed a lower Φ_{PSII} than mature ones in both HW and C leaves ($p = 0.035$; Fig. 3). No significant differences were found between HW and C leaves nor between tissue ages during the heatwave recovery.

Oxidative stress. There was no significant variability in the concentration of oxidative stress indicators in *C. nodosa*'s leaf tissues between treatments HW and C (Table 2).

Although non-significant, total phenols and MDA concentration were slightly higher in HW leaves than C leaves during the heatwave, whereas TEAC and ORAC concentrations were slightly lower in HW leaves than control. On the other hand, total phenols, TEAC, ORAC, and MDA concentrations were slightly higher in HW leaves than control during the heatwave recovery.

Leaf area vs dry weight ratio. *C. nodosa*'s leaf area *vs* DW ratio was significantly higher in HW than C leaf tissues during the heatwave recovery (Fig. 4). Hence, for the same leaf area, *C. nodosa*'s leaves that went through a heatwave simulation had less biomass than those grown in control conditions.

Discussion

Our results show that MHWs (in this case, a seven-day spring heatwave peaking at 28 °C) have a negative impact on *C. nodosa*'s physiology, but the effects may only become evident in the aftermath of the heatwave peak. Reduction of the photosynthetic capacity and light-saturating irradiance was observed 7 days after the end of the heat stress, along with a decrease in leaf biomass. Coupled to the reduced photosynthetic rates and efficiency, this leaf biomass loss implies an additional reduction of the global productivity of the plants, with direct consequences

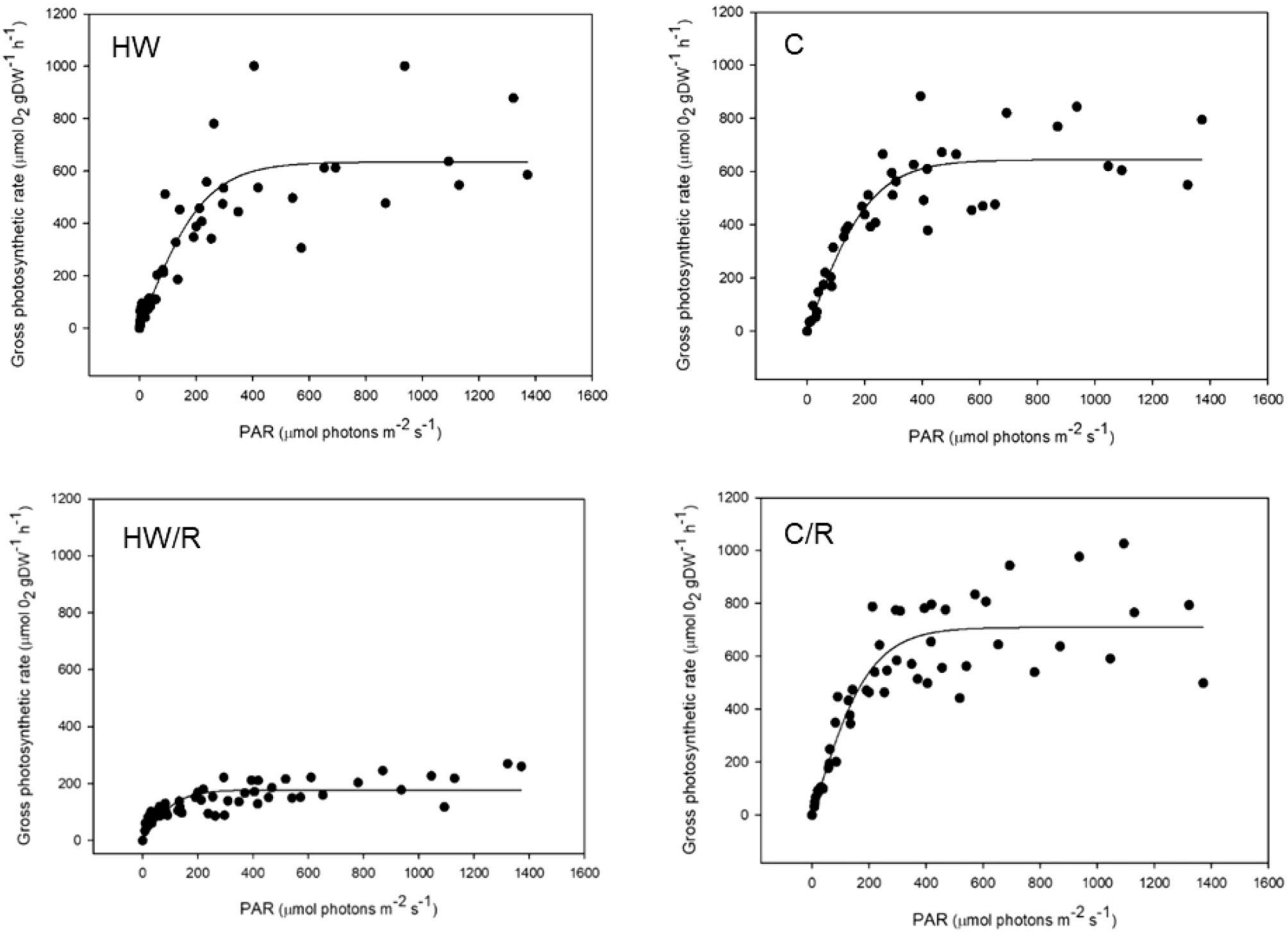

Figure 1. P-I curves of *C. nodosa*'s leaves. Leaves were sampled during the heatwave peak (heatwave, HW, and control, C) and after a 7-day recovery (HW/R and C/R). Data were fitted with the Jassby & Platt (1976) model equation.

Treatment	Parameters				
	α ± SE	P_m ± SE	I_k ± SE	R^2	*n*
Heatwave					
HW	2.805 ± 0.352	635.02 ± 37.05	226.4 ± 31, 3	0.809	55
C	2.921 ± 0.305	644.9 ± 27.5	220.8 ± 24.9	0.856	44
Significance level	n.s	n.s	n.s		
Heatwave recovery					
HW	1.429 ± 0.229	177.4 ± 8.1	124.2 ± 20.7	0.661	54
C	3.539 ± 0.372	709.8 ± 27.6	200.6 ± 22.5	0.841	55
Significance level	***	***	*		

Table 1. *C. nodosa's* photosynthetic parameters obtained after fitting the data with the Jassby & Platt (1976) P-I model. Mean photosynthetic quantum efficiency (α; µmol O_2 gDW^{-1} h^{-1}/µmol photons m^{-2} s^{-1}), maximal photosynthetic rate (P_m; µmol O_2 gDW^{-1} h^{-1}), and half-saturation irradiance (I_k; µmol photons m^{-2} s^{-1}) are expressed as values ± SE, for each treatment, with corresponding R^2 and number of observations (*n*). The significance level is the degree of significant difference between treatments HW and C (n.s.: non-significant; *: significant, $p < 0.05$; ***: highly significant, $p < 0.001$), both during the heatwave and after heatwave recovery.

on growth. On the other hand, the heatwave did not imply significant oxidative damage or changes in the leaves' antioxidant system of *C. nodosa*.

While the heatwave peak only affected Φ_{PSII} significantly, the measured photosynthetic parameters showed a strong decrease after 7 days of recovery at lower temperature: the maximal photosynthetic rate (P_m), the amount of O_2 released per unit of incident light (α) and the minimum-light intensity needed to reach P_m (I_k)

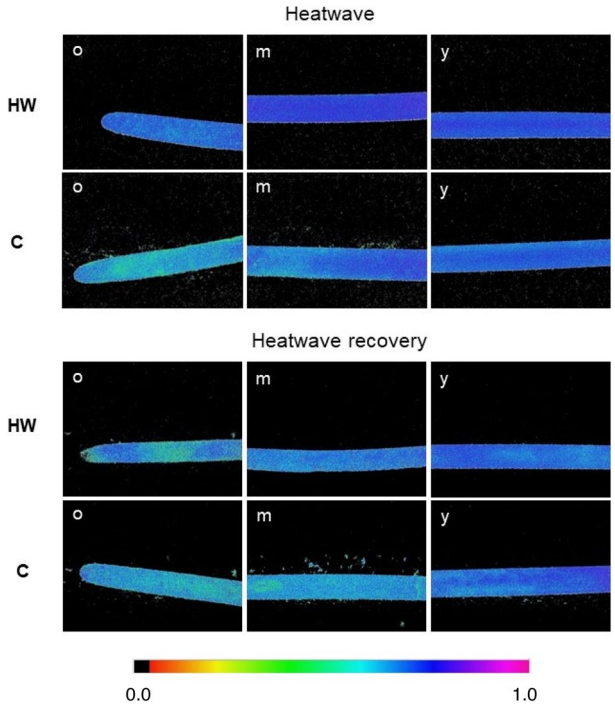

Figure 2. Examples of CFI pictures of *C. nodosa*'s Φ_{PSII}, after a saturating light pulse. CFI was done on mature leaves sampled from shoots cultivated in heatwave (HW) and control (C) conditions, both during the heatwave and after heatwave recovery. o, m and y indicate different leaf parts (old, mature and young, respectively). Colour bar on the bottom indicates Φ_{PSII} values ranging from 0.0 (black) to 1.0. (pink). Pictures are 24 × 32 mm (6 × magnification).

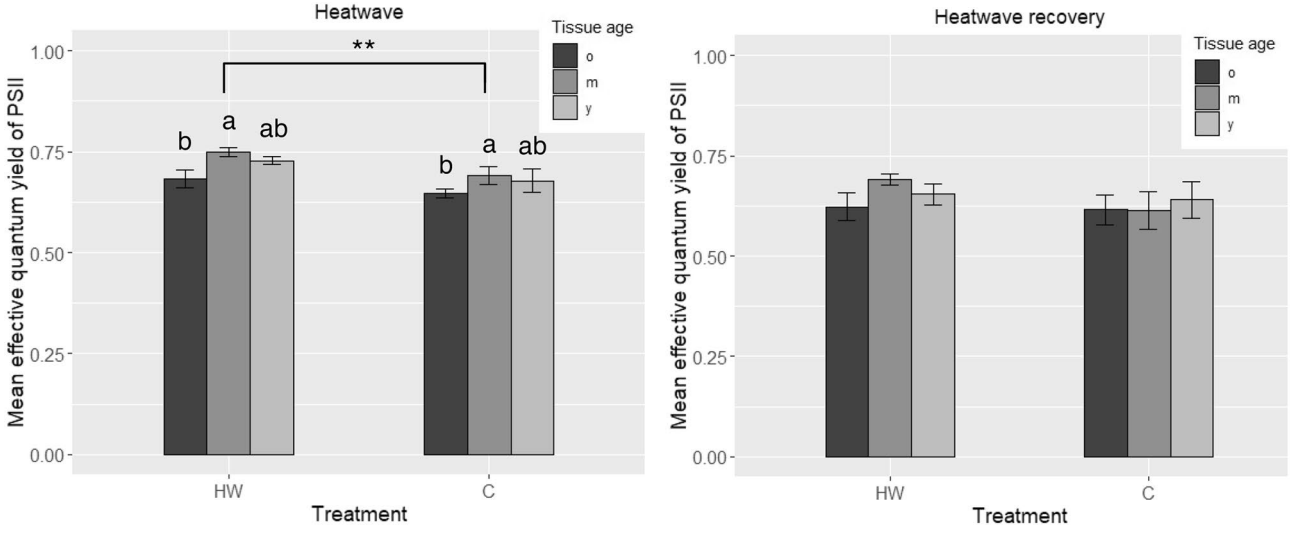

Figure 3. Effective quantume yield of PSII (Φ_{PSII}) of *C. nodosa*'s leaf tissues. Old (o), mature (m) and young (y) leaf tissues were sampled from shoots cultivated in heatwave (HW) and control (C) conditions, both during the heatwave and after heatwave recovery. Values are mean ± SE ($n = 5$). Different letters indicate significant differences between tissue ages ($p < 0.05$), and ** indicates significant differences between treatments HW and C ($p < 0.01$).

dropped significantly during the recovery period. Conversely, no changes in these photosynthetic parameters were observed during the heatwave, showing that the effects only became apparent several days after the alleviation of the heat stress. Φ_{PSII} increased significantly during the heatwave, accounting for a higher electron transport rate in the electron transport chain of photosynthesis[44] under the heat stress provoked by the MHW. Maintaining a high electron flow in the electron transport chain is advantageous to compensate the negative effects of heat stress and keep photosynthetic and growth rates at a constant level. Φ_{PSII} was higher in mature parts of the leaves

	Treatment			
	Heatwave		*Heatwave recovery*	
	HW	C	HW	C
Total phenols (mg gDW^{-1})	11.81 ± 1.72	10.93 ± 0.23	10.79 ± 0.92	10.17 ± 1.41
	n = 5	*n* = 4	*n* = 5	*n* = 5
TEAC (µmol Trolox eq gDW^{-1})	9.47 ± 3.48	9.95 ± 3.09	12.22 ± 1.36	7.96 ± 1.83
	n = 5	*n* = 5	*n* = 5	*n* = 5
ORAC (µmol Trolox eq gDW^{-1})	139.24 ± 34.32	206.01 ± 62.66	132.27 ± 51.08	126.98 ± 13.46
	n = 5	*n* = 5	*n* = 5	*n* = 5
MDA (nmol gDW^{-1})	88.71 ± 20.81	83.49 ± 20.62	186.58 ± 2.14	100.85 ± 34.09
	n = 4	*n* = 4	*n* = 3	*n* = 5

Table 2. Total phenols (mg gDW^{-1}), TEAC (µmol Trolox eq gDW^{-1}), ORAC (µmol Trolox eq gDW^{-1}) and MDA (nmol gDW^{-1}) concentrations in mature *C. nodosa*'s leaves from heatwave (HW) and control (C) tanks, during the heatwave and after recovery. Values are means ± SE and *n* is the number of replicates.

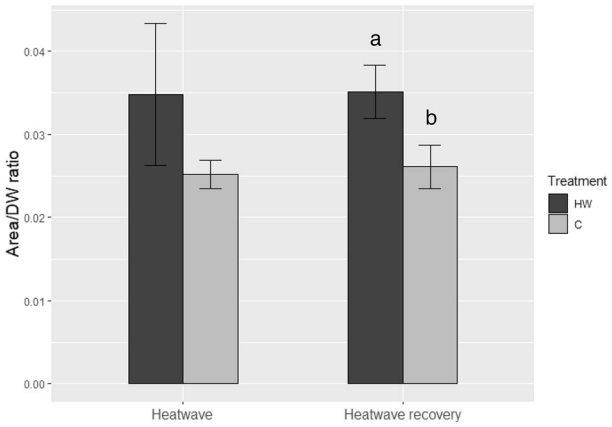

Figure 4. Area *vs* dry weight (DW) ratio of *C. nodosa*'s leaf tissues. Leaf tissues from shoots cultivated in heatwave (HW) and control (C) conditions were sampled both during the heatwave and during heatwave recovery. Values are means ± SD ($n = 5$). Different letters indicate significant differences ($p < 0.01$).

than in old tissues, which has been shown to be a common feature related to the reduction of leaf thickness and cell layers towards the tip[45]. Nonetheless, in our work, this feature was not noticeable during heatwave recovery, which may be related to the increased area *vs* DW ratio in heatwave recovering leaves, as discussed below. When Φ_{PSII} returned to control level several days after heatwave relief, the photosynthetic performance of the plant dropped, suggesting that *C. nodosa* is only able to temporarily maintain its gross photosynthetic activity at a normal rate under thermal stress as a "compensation" response, by increasing the electron transport rate through PSII during a few days. However, it is likely to be unable to sustain this metabolic compensation response in the long term, resulting in the drop of photosynthetic performance several days after the heat stress, while Φ_{PSII} drops back to control level. Costa et al. also suggested that Φ_{PSII} increases with heat stress in *C. nodosa* leaves (after a 4-day heat shock at 40 °C)[35]. This study confirms that a short-term response to heat stress involves an increase in Φ_{PSII}, probably to support photosynthesis during thermal stress. The fact that Φ_{PSII} returns to control levels after the heatwave suggests that *C. nodosa*'s PSII has a certain ability to recover from the heat-stress damage[39]. However, nothing suggests that it would be able to recover from a more intense and long-lasting MHW, as those forecasted in future climate-change scenarios. Costa et al. also suggested that P_m was lower in *C. nodosa* shoots that had suffered from intense thermal stress (4 days at 40 °C) than in plants kept at 20 °C[35]. While both a 4-day heat shock at 40 °C and our 7-day heatwave at 28 °C had negative consequences on the photosynthetic activity of *C. nodosa* in Ria Formosa, the responses seem to appear at different time scales (right after the heat shock and after a 7-day recovery, respectively). We suggest that a prolonged, but less intense temperature rise (namely the MHW), may have delayed consequences on the plant's photosynthetic activity, whereas a short, although more intense heat stress, involves an immediate decrease of P_m, and with it, the immediate drop of photosynthetic efficiency. Yet, the resilience of *C. nodosa* to MHWs must be investigated on a longer time scale (e.g., after a more extended recovery period) to know whether this species can entirely recover from the heatwave or if such consequences are irreversible.

The unchanged photosynthetic parameters, together with the increase in Φ_{PSII} in leaves during the heatwave, may be related with the increase of O_2-independent electron flow, such as the cyclic electron flow within PSII, or the water-water cycle (PSI) that does not imply net O_2 uptake while regenerating the ascorbate needed for

antioxidant protection[46] and allowing extra ATP synthesis. The decrease of photosynthetic performance in heatwave-recovering leaves suggests that a higher fraction of the oxygen produced by photosynthesis is consumed during the heat stress recovery, indicating the up-regulation of the oxygen-consuming process(es), such as respiration and photorespiration[47,48]. The increment of these oxygen-consuming processes can in turn enhance the production of reactive oxygen species (ROS) such as H_2O_2 and superoxide radicals[49,50]. Although it has been reported that thermal stress induces the production of ROS in submerged macrophytes[51], the putative consequences of increased oxidative stress were not observed here, as neither membrane lipid peroxidation (measured as MDA) nor the ROS scavenging capacity (TEAC and ORAC) presented significant changes during and after the heatwave. Similarly, the unchanged MDA values show that the possible increase in ROS did not provoke oxidative stress, meaning that the existing antioxidant system of *C. nodosa* was probably sufficient to avoid oxidative damage. Yet, we cannot entirely rule out the possibility that stress was not detected due to putative limitations of the parameters analysed.

Although non-significantly, total phenols, TEAC, ORAC and MDA concentrations were slightly higher in leaves recovering from the MHW than in control ones. While the short-term effects of the heatwave on biochemical oxidative-stress indicators were not clearly shown in this experiment, the consequences appear to be more relevant during the recovery. This could be interpreted as a long-term acclimation response of *C. nodosa*'s biochemistry to the potentially low oxidative stress caused by the prolonged heat stress. Costa et al. suggested that a short and intense heat stress (40 °C for 4 days) implies a significant increase in *C. nodosa*'s antioxidant response (measured with TEAC)[35]. The non-significance of our results may be justified by the characteristics of the MHW or heat shock, which, in the same study, was more intense and suddenly imposed, whereas in the present work, the MHW was progressively imposed and less intense. The absence of oxidative damage (measured with MDA) under a short and intense heat shock[35] is in line with our results. Indeed, MDA concentration did not increase in *C. nodosa* leaves exposed to thermal stress, suggesting that *C. nodosa* is resistant to the stress caused by MHWs of different lengths and intensities. Nonetheless, foliar MDA is slightly higher after recovery from a prolonged heatwave (ca. 190 nmol gDW^{-1}; present study) than right after a short and intense heat shock (ca. 100 nmol gDW^{-1}[35]). These results suggest that oxidative damage is likely to be more important in plants recovering from heatwave-type stress (more extended heat stress, long-term effect) than immediately after a short heat shock. In Ria Formosa, *C. nodosa* seems to have a sufficient antioxidant capacity to cope with stress induced by a spring MHW. Yet, a longer and/or more severe MHW for this time of the year may eventually significantly increase the oxidative stress and cell damage in *C. nodosa* leaves.

This study showed that the simulated MHW also impacted the morphology of *C. nodosa*'s leaves, by inducing a decrease in leaf biomass, especially several days after the end of the heatwave, as shown by changes in the area *vs* DW ratio. *C. nodosa* might have responded to the thermal stress by a reduction in its leave's thickness, which could be explained by a lower photosynthetic performance and, therefore, a lower growth rate. Another possibility is the increase of the size of the aerenchyma. Aerenchyma lacunae act as either sources or sinks for O_2[52,53], and an increase in their volume could be related to a higher O_2 transfer inside the plant, (from leaves to roots and rhizomes) together with enhanced electron transport (as seen before) or stand for more intense gas exchange for respiration/photorespiration processes. Cross-section analysis of *C. nodosa*'s leaves[45] would be helpful to further investigate the effect of MHWs on the leave's anatomy and, more precisely, observe changes in the size of the aerenchyma[54,55].

The present study investigated the effects of a particular spring-like MHW in Ria Formosa on *C. nodosa* shoots. Results must not be extrapolated for all-year-round conditions or for shoots coming from different thermal environments (temperate or tropical/subtropical). In fact, the optimum temperature for seagrass growth and photosynthesis does not only varies between species but also between individuals of the same species coming from different origins[41], and metabolic responses of the plants to MHWs can greatly vary with their historic thermal environment[31,34,56,57]. Also, seagrasses may have different responses to MHWs, whenever these events occur at different times of the year (summer/winter), as the plant's metabolism follows a seasonal pattern[58]. In the case of reoccurrence of MHW events in a relatively short time, *C. nodosa* and other seagrass species are likely to be more susceptible and more critically affected by heat stress. In fact, Saha et al. showed that cumulative heatwave events have a negative impact on the growth and leaf production rate (*i.e.*, biomass) of *Z. marina,* whereas an isolated MHW event did not induce any significant change in the plant's biology[59].

Overall, studies show that *C. nodosa* seems to present a higher tolerance to anomalous temperature events than other seagrass species in the same thermal environment[28,38,56,60]. Although *C. nodosa*'s optimal temperatures are higher than other seagrass species, a spring-like heatwave such as the one simulated in the present work have the potential to negatively impact *C. nodosa* population in Ria Formosa if occurring during a period when seasonal temperatures are lower (e.g., in autumn or early spring). Investigate MHWs' effects at different times of the year is thus needed to test this hypothesis. In the complex nature realm, an array of biotic and abiotic parameters interacts with the potential to induce synergistic or antagonistic effects[61,62]. Hence, analysing the effects of one parameter (here, the temperature) does not necessarily allow forecasting one species' response in its natural environment, and conclusions must be withdrawn with caution. Although temperature is the most important factor affecting its production, *C. nodosa* expresses a large variety of responses to different combinations of factors[63]. Therefore, multifactorial experiments are needed to predict more accurately the responses of seagrasses to environmental stressors, like temperature. Finally, comparisons with previous studies must be taken carefully because of the lack of homogenization in methodologies and experimental designs.

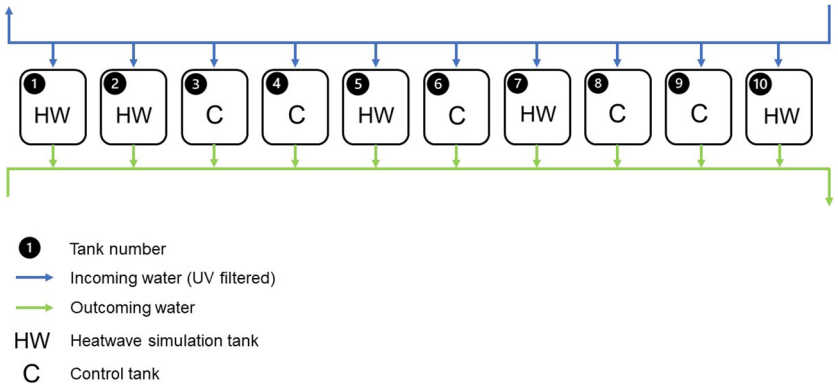

Figure 5. Schematic representation of the experimental setup. Tank number, random treatment assignation (Control, C and Heatwave, HW) and water flow direction (open circuit).

Methods

Study site. The Ria Formosa coastal lagoon, located in the south coast of Portugal (36°58'N, 8°02'W to 37°03'N, 7°32'W), is an 84 km^2 shallow mesotidal lagoon. It has been a Natural Park since 1987 and is a Ramsar and Natura 2000 protected area. It is one of the most important wetlands in Europe, spanning over 55 km long and a maximum of 6 km width[64]. The lagoon is 2 m deep on average, and its tidal amplitude varies between 3.50 m on spring tides and 1.30 m on neap tides[65]. It is separated from the Atlantic Ocean by five dynamic barrier islands and two peninsulas and is linked to it by seven channels, five natural and two artificial, allowing water exchange with the ocean. Essentially composed of salt marshes and mudflats in the intertidal and shallow channels in the subtidal, the highly productive Ria Formosa hosts a rich diversity of fauna and flora. It is an important nursery hotspot and feeding ground for many fish and mollusc species[66], which gives the lagoon high ecological importance. Mean air temperature is 25 °C in summer and 12 °C in winter, which gives Ria Formosa a Mediterranean climate, despite being situated on the Atlantic coast[64]. In this mesotidal system, May–June seawater temperature commonly ranges between 18 °C and 30 °C (https://www.hidrografico.pt/boias). However, in intertidal pools and shallow subtidal areas, the thin water column (especially during low spring tides), coupled to high air temperature and high irradiance, drives the water temperature to rise dramatically, especially in summer[29] when it can reach 35 °C (João Silva, personal communication). Such drastic environmental changes can significantly affect the physiology and survival of most species found in the Ria Formosa, including seagrasses.

Plant collection. *C. nodosa* plants, including rhizomes, roots, apical meristem, and shoots with 3–4 leaves each, were carefully collected in Ria Formosa's Ramalhete channel on May 3rd, 2021 (Supplementary Fig. S1). Following collection, shoots were kept in seawater in closed dark tanks until transplantation into a mesocosm facility within 24 h of uprooting. The collection and use of seagrasses and other plants for experimental purposes in Ria Formosa Natural Park is regulated by ICNF (Institute for Nature Conservation). Therefore, in order to comply with national legislation, a permit (Licença nº17/2021/Recolha) was issued for the collection of all the plant material used in this study. All methods were carried out in accordance with relevant national and international guidelines. A voucher specimen was deposited in the Herbarium of Universidade do Algarve (ALGU) with accession number 15779.

Experimental setup. An indoor mesocosm experiment was conducted in the Ramalhete station. Ten 65-L plastic tanks (5 replicates per treatment, $n = 5$) were filled with 15 cm of sand collected from Faro beach and supplied with water pumped from Ria Formosa through an open circuit (Supplementary Fig. S2). To reduce microalgae development and contamination in the facility, water pumped from Ria Formosa flowed through a 50-W UV filter before entering the circuit. The water temperature in the circuit was controlled with a temperature controller (ECLI20MA IKOMFORTRC900 inverter, i-Komfort, Kripsol, Toledo, Spain). It flowed into the aquaria at 14 L h^{-1} and was entirely renewed every 5 h. The aquaria were aerated with a bubbling air pipe, and water was kept in motion and homogenised with a water fan. The light above each tank was provided by LED lamps (Ledvance Flood LED 50 W/6500 K WT, Augsburg, Germany) hung above each tank in such a way as to provide approximately the same light intensity in the spectral range from 400 to 700 nm to each aquarium. Light intensity in this spectral range was measured and calibrated before starting the experiment with an LI-250A Light Meter and an LI-190R sensor (LiCor, USA) and ranged from 101.6 to 130.8 µmol m^2 s^{-1} (113.2 µmol m^2 s^{-1} on average) just on top of the water surface. To simulate the natural conditions, the lights were automatically turned on at 6 a.m. and off at 9 p.m. (light: dark photoperiod of 15 h: 9 h). The day following harvesting, *C. nodosa* shoots were carefully cleaned from epiphytes and 25 shoots were placed in each aquarium under controlled light and temperature conditions.

Two treatments (control, C and heatwave, HW) were randomly assigned to the aquaria (Fig. 5).

After the transplant, shoots were left 33 days at 20 °C (1 °C above the water temperature during collection) to allow the plants to acclimate to their new environment. While the C aquaria were kept at 20 °C during the experiment, the MHW simulation was applied in the HW aquaria. The temperature was daily monitored throughout the

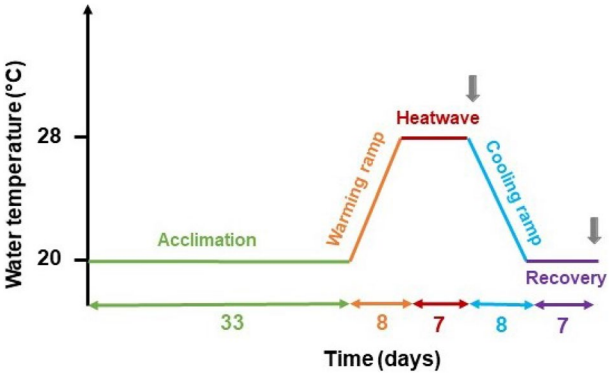

Figure 6. Scheme of the experimental schedule. Water temperature as a function of time. *Acclimation*, *warming ramp*, *heatwave*, *cooling ramp*, *recovery,* and respective duration on the x-axis (in days). Grey arrows indicate the two sampling times.

experiment in all tanks, at the warmest time of the day (between 2 p.m. and 4 p.m.), with a manual thermometer. The temperature was monitored and controlled during the heatwave simulation in each of the five HW tanks with a temperature controller (AquaMedic T controller twin, Bissendorf, Germany).

Heatwave characteristics. Determination of the maximum temperature (T_{max}) of the simulated MHW was based on previous in situ temperature records and the definition of MHWs given by Hobday et al.[67,68]. Temperature data previously recorded in *Caulerpa prolifera* beds (mean daily temperature data, from 10–06-2017 to 17–06-2019; de los Santos, personal communication) was used to get a proxy of the yearly temperature in *C. nodosa* beds in Ria Formosa, as both species are found at a similar depth[69].

To assess the oceanic SST and the occurrence of oceanic MHWs in Ria Formosa, the NOAA Optimum Interpolation Sea Surface Temperature (OISST) dataset (Huang et al.; methodology developed by Reynolds et al. and described by Banzon et al.)[70–72] was used. The daily temperature dataset, displayed on the Marine Heatwaves Tracker app[73], contains the oceanic sea surface temperature (SST), climatology, threshold[67] data and the MHW events record from 1982 to the present day. A pixel close to Ria Formosa's inlet channel (Lon = 7.875°W, Lat = 36.875°N) was selected, and a time series was plotted for the oceanic SST from 10–06-2017 to 17–06-2019 (Supplementary Fig. S3).

To determine the temperature inside Ria Formosa during a heatwave event and the potential difference to oceanic MHWs, the correlation between the temperature inside and outside Ria Formosa was established for the year 2018 ($R^2 = 0.885$; Supplementary Fig. S4), and the SST climatology inside Ria Formosa was then extrapolated (Supplementary Fig. S5). The occurrence of oceanic MHWs close to Ria Formosa for this time of the year was prospected in the historical data available at the Marine Heatwaves Tracker website (Supplementary Fig. S6). At his location, MHWs happen at any time of the year and have been intensifying in the last decade. MHW events in the Ria Formosa area in the past years during the April-June period were of Moderate intensity (category I; MHWs classification by Hobday et al.)[68]. Nonetheless, there is a global trend toward the increasing frequency of Strong intensity (category II) MHWs[68]. Moreover, the temperature in Ria Formosa's shallow areas can increase dramatically (João Silva, personal communication) until locally reaching the temperature corresponding to MHWs of Severe and Extreme intensity (category III and IV). An event of Extreme intensity was chosen in this experiment to simulate the dramatically high temperatures of shallow waters and observe its impacts on the seagrass' metabolism, as a simulation of what is likely to happen in the future according to the MHWs prediction scenarios[74].

Following the heatwave characterisation and classification proposed by Hobday et al.[68], an MHW of Extreme intensity (category IV) is characterised by a peak temperature reaching at least 4 × the 90th percentile difference from the mean regional climatology value. We applied this principle to the extrapolated Ria Formosa's temperature dataset (Supplementary Fig. S7). Between April 1st and June 30th, an MHW of Extreme intensity in Ria Formosa peaks at least at 25.9 °C. However, as said before, water temperature can increase dramatically above this value in some shallow areas of Ria Formosa, such as the smaller channels. Hence, choosing 28 °C as the peak temperature is relevant to simulate an Extreme-intensity MHW in Ria Formosa's shallow water conditions.

According to the definition given by Hobday et al.[67] a MHW has a duration of at least 5 days. Hence, the MHW simulated in this experiment was designed with a seven-day duration and a peak temperature of 28 °C to simulate a spring-like MHW event of Extreme intensity in Ria Formosa's shallow channels. The experiment's timeline is described in Fig. 6. After the acclimation period, water temperature was increased from 20 °C to 28 °C, by 1 °C a day during eight days ("*warming ramp*"), maintained at 28 °C for seven days ("*heatwave*"), and then decreased back to 20 °C by 1 °C a day ("*cooling ramp*"). Then, plants were allowed to recover from the heatwave for seven days at 20 °C ("*heatwave recovery*").

Sampling design. Samples were collected from each tank (HW, $n = 5$ and C, $n = 5$) at the end of the heatwave peak ("*heatwave*") and at the end of the recovery period ("*recovery*"; Fig. 6).

Whole mature leaves (the 2nd or 3rd youngest leaf from each shoot) were collected for CFI analysis. The middle part of mature leaves was collected for P-I curves, biochemical analysis, and to calculate the area *vs* DW ratio.

Photosynthesis-Irradiance (P-I) response curves and Chlorophyll fluorescence imaging (CFI). P-I curves ($n = 4$) were performed accordingly to Silva et al.[75], after the heatwave peak (HW, C) and after heatwave recovery (HW/R, C/R). The setup, installed right next to the mesocosm facility, was composed of five independent chambers, each with a round plastic PVC chamber filled with water from the aquaria and sealed with a petri dish containing an optical O_2 sensor (Presens Spot PS; Supplementary Fig. S8).Water temperature inside the chambers was kept at 28 °C (HW) and 20 °C (C, HW/R, C/R) by a closed-circuit thermostatic water-bath temperature controller (Julabo HC, Julabo Labortechnik, Seelbach, Germany). A magnetic stirrer ensured water homogenisation inside the chambers. Light energy was provided by five LED lamps, whose irradiance was previously measured with a Li-Cor LI-190 cosine quantum sensor (LI-COR, Lincoln, NE, USA). Combinations of neutral density filters were used to obtain the different light intensities needed. Leaf samples were cleaned from epiphytes; the middle part was cut into 3 segments (≈ 5 cm long) and then placed side by side inside the chambers to ensure their even exposure to light. Leaf segments were incubated inside the chambers under increasing photosynthetically active radiation (PAR), with ten light levels ranging from 0 to 1372 µmol photons m^{-2} s^{-1}. Light intensities used for measurements were chosen beforehand to draw an accurate P-I curve shape. O_2 concentration (µmol L^{-1}) was measured in each chamber, firstly after 20–30 min incubation in the dark (dark respiration, DR) and then under each light intensity (net photosynthesis, NP) with a Microx 4 PreSens Optode (Regensburg, Germany). Photosynthetic rates (DR, NP (1) and GP (2); µmol O_2 gDW^{-1} h^{-1}) were calculated as follows:

$$DR, NP = \frac{\frac{[O_2]_f - [O_2]_i}{T} \times V}{DW} \quad (1)$$

where $[O_2]_f$ = Final O_2 concentration (µmol L^{-1}); $[O_2]_i$ = Initial O_2 concentration (µmol L^{-1}); T = Incubation time (h); V = Volume of the chamber (L); DW = Dry weight of the leaf tissue (g)

$$GP = NP + DR \quad (2)$$

O2 saturation levels were periodically checked during the measurements, and incubation time was adjusted to avoid O_2 supersaturation in the chamber, which can inhibit photosynthesis and involve pH changes[54,76]. GP response to PAR was analysed using the Jassby & Platt model[77,78] with SigmaPlot for Windows (version 14.0, 2017 Systat Software, Inc.). Maximum photosynthetic rate ($P_{m;}$ µmolO_2 gDW^{-1} h^{-1}) and photosynthetic efficiency (α; µmolO_2 gDW^{-1} h^{-1}/µmol photons m^{-2} s^{-1}) were calculated from the Jassby & Platt fit model, and the half-saturation irradiance ($I_{k;}$ µmol photons m^{-2} s^{-1}) was calculated according to the following equation:

$$I_k = \frac{P_m}{\alpha} \quad (3)$$

CFI was done right after leaves sampling with an IMAG-K2 Imaging-PAM Fluorometer (M-Series Chlorophyll Fluorescence System, WALZ, Germany). A 0.8 s saturating light pulse (ca. 5000 µmol photons m^{-2} s^{-1}) was applied to each sample immediately before taking the image. Φ_{PSII} is widely used to assess the level of plant stress in seagrasses [54], as is it highly sensitive to stress. Φ_{PSII} in ambient light conditions was computed from each image by "point measurements", according to the following equation[79] :

$$\Phi_{PSII} = (F'_m - F_s)/F'_m = \Delta F/F'_m \quad (4)$$

where F'_m: Maximum fluorescence of the light-adapted leaf tissue; F_s: Steady-state fluorescence of the light-adapted leaf tissue.

For each leaf sampled, three images were taken, one per tissue age (*young*, *mature* and *old*). For each tissue age, three replicates of areas of interest (AOI) were selected on the leaf's image to calculate mean Φ_{PSII}.

Total phenolic content (TPC), Trolox® equivalent antioxidant activity (TEAC), oxygen radical absorbance capacity (ORAC) and malondialdehyde (MDA) quantification. Foliar antioxidant biochemical indicators (Total Phenolic Content, TPC, Trolox® Equivalent Antioxidant Capacity, TEAC, and Oxygen Radical Absorbance Capacity, ORAC) and oxidative damage (Malondialdehyde, MDA) were investigated. Following collection, leaf samples were carefully cleaned from epiphytes, rinsed with distilled water, blotted dry, frozen in liquid nitrogen, and stored at – 80 °C until analysis.

TPC, TEAC and ORAC were quantified according to Costa et al.[35]. 0.15 g of frozen leaf samples were powdered in liquid nitrogen, suspended in 2.5 mL of hydrochloric acid (HCL) 0.1 N, kept overnight in the dark under constant shaking at 4 °C, and then centrifuged (4700 xg, 30 min, 4 °C). The supernatant was used to quantify TPC and for TEAC and ORAC assays.

TPC was quantified using the Folin-Ciocalteu method[80,81]. 42 µL of the phenolic extract was added to 0.4 mL Folin-Ciocalteu reagent 0.25 N and 0.4 mL of NA_2CO_3 7.5%. Absorbance was read at 724 nm (Novaspec Plus, Healthcare Bio-Sciences AB, Uppsala, Sweden). Chlorogenic acid was used as a standard, and TPC was expressed as chlorogenic acid equivalents.

The TEAC assay quantifies the protection capacity against peroxyl radicals (ROO•) through total antioxidant capacity based on a single electron transfer. A cation radical $ABTS^{\bullet+}$ solution was produced by adding 7 mM ABTS to potassium persulfate (2.45 mM final concentration), according to Re et al.[82]. 990 µL of diluted

$ABTS^{\bullet+}$ solution (absorbance 0.8 ± 0.02 at 734 nm) was added to 10 µL of extract and read at 734 mm (Novaspec Plus, Healthcare Bio-Sciences AB, Uppsala, Sweden). Results were expressed as Trolox® (6-Hydroxy-2,5,7,8-tetramethylchromane-2-carboxylic acid) equivalents.

The ORAC assay quantifies the protection capacity against peroxyl radicals through hydrogen atom transfer (HAT). The ORAC analysis was done following Gillespie et al.[83] and Huang et al.[84], and using ABAP [2,2′-azobis (2-methylpropionamidine) dihydrochloride] instead of AAPH [2,2′-azobis(2-amidinopropane) dihydrochloride] as a lipophilic peroxyl radical generator. 150 µL of 8.2×10^{-5} mM fluorescein in 75 mM potassium phosphate buffer (pH 7.4) was added to 25 µL of extract, heated to 37 °C and read in a Synergy TM 4 multi-detection microplate reader (485 nm excitation filter, 20 nm bandpass, and 528 nm excitation filter, 20 nm bandpass). The reaction was initiated by adding 25 µL of freshly prepared 153 mM ABAP. The results were expressed as Trolox® equivalents.

MDA is a final secondary product of polyunsaturated fatty acids autooxidation (responsible for cell damage) and enzymatic degradation. Hence, it is considered a valuable indicator of lipid peroxidation under oxidative stress[85]. MDA extraction and quantification was performed as in Hodges et al.[85]. 300 mg of frozen leaf tissue were ground in liquid nitrogen and suspended in 5 mL ethanol 80%. After homogenization, the extracts were centrifuged at 3000xg for 10 min. 1 mL of supernatant was added to 1 mL of 20% trichloroacetic acid (TCA) with 065% thiobarbituric acid (TBA) and 0.015% butylated hydroxytoluene (BHT) solution. Two blank solutions were made without TBA or with ethanol 80% instead of sample extract. After mixing well, all samples and blanks were incubated at 90 °C for 25 min, cooled down in ice for 15 min, and centrifuged at 3000 xg for 10 min. The supernatant absorbances were read at 440, 532 and 600 nm (Novaspec Plus, Healthcare Bio-Sciences AB, Uppsala, Sweden), and MDA equivalents were calculated as in Hodges et al.[85].

Leaf area vs dry weight ratio. Leaves' area *vs* dry weight (DW) ratio was calculated. Leaf segments were photographed for later measurement of their surface area (m^2) with the ImageJ software[86] and each sample's DW was measured after drying at 60 °C for at least 48 h.

Statistical analyses. All statistical analyses were performed using R Studio software[87]. Beforehand, data were tested for normality (Shapiro–Wilk's test) and homogeneity of variances (Levene's test). Differences between treatments (HW *vs* C) at both sampling times ("*heatwave*" and "*heatwave recovery*") were tested using one-way analysis of variance (ANOVA). Whenever the hypothesis of homogeneity of variance was rejected, a Welch ANOVA test was performed, followed by a Games-Howell post-hoc test. To investigate the coupled effects of tissue age and treatment on Φ_{PSII}, a two-way ANOVA was performed. In case of the absence of significant interaction between the two factors, two one-way ANOVAs were performed to search for any significant difference in Φ_{PSII} between leaf parts and between treatments, independently. If significance was detected, a Tukey-HSD test was performed for pairwise comparison of the factors "leaf part" and "treatment". For all tests, a significance level of $\alpha = 0.05$ was used. Data points that deviated from the upper and lower quartiles more than 1.5-fold the interquartile range were considered outliers and were not included in the analysis[88].

Data availability

The datasets generated and/or analysed during the current study are not publicly available due to confidentiality reasons, but are available from the corresponding author on reasonable request.

Received: 9 February 2022; Accepted: 5 May 2022
Published online: 13 May 2022

References

1. IPCC: IPCC Special Report on the Ocean and Cryosphere in a Changing Climate [Pörtner, H.-O. *et al.*] In press (2019).
2. Oliver, E. C. J. *et al.* Longer and more frequent marine heatwaves over the past century. *Nat. Commun.* **9**, 1324 (2018).
3. Gibble, C. *et al.* Investigation of a largescale Common Murre (*Uria aalge*) mortality event in California, USA, in 2015. *J. Wildl. Dis.* **54**, 569–574 (2018).
4. Brodeur, R. D., Auth, T. D. & Phillips, A. J. Major shifts in pelagic micronekton and macrozooplankton community structure in an upwelling ecosystem related to an unprecedented marine heatwave. *Front. Mar. Sci.* **6**, 212 (2019).
5. Le Nohaïc, M. *et al.* Marine heatwave causes unprecedented regional mass bleaching of thermally resistant corals in northwestern Australia. *Sci. Rep.* **7**, 1–11 (2017).
6. Hughes, T. P. *et al.* Global warming transforms coral reef assemblages. *Nature* **556**, 492–496 (2018).
7. Genevier, L. G., Jamil, T., Raitsos, D. E., Krokos, G. & Hoteit, I. Marine heatwaves reveal coral reef zones susceptible to bleaching in the Red Sea. *Glob. Change Biol.* **25**, 2338–2351 (2019).
8. Leggat, W. P. *et al.* Rapid coral decay is associated with marine heatwave mortality events on reefs. *Curr. Biol.* **29**, 2723–2730 (2019).
9. Green, E. P. & Short, F. T. *World Atlas of Seagrasses* (University of California Press, 2003).
10. Duarte, C. M. The future of seagrass meadows. *Environ. Conserv.* **29**, 192–206 (2002).
11. Alongi, D. M. *Blue Carbon: Coastal Sequestration for Climate Change Mitigation* (Springer, Berlin, 2018).
12. Blandon, A. & ZuErmgassen, P. S. Quantitative estimate of commercial fish enhancement by seagrass habitat in southern Australia. *Estuarine Coast. Shelf Sci.* **141**, 1–8 (2014).
13. Boudouresque, C. F., Mayot, N. & Pergent, G. The outstanding traits of the functioning of the *Posidonia oceanica* seagrass ecosystem. *Biol. Mar. Medit.* **13**, 109–113 (2006).
14. Carr, J., D'odorico, P., McGlathery, K. & Wiberg, P. L. Stability and bistability of seagrass ecosystems in shallow coastal lagoons: Role of feedbacks with sediment resuspension and light attenuation. *J. Geophys. Res. Biogeosci.* https://doi.org/10.1029/2009JG001103 (2010).
15. Welsh, D. T. Nitrogen fixation in seagrass meadows: regulation, plant–bacteria interactions and significance to primary productivity. *Ecol. Lett.* **3**, 58–71. https://doi.org/10.1046/j.1461-0248.2000.00111.x (2000).
16. Duarte, C. M. *et al.* Seagrass community metabolism: Assessing the carbon sink capacity of seagrass meadows. *Glob. Biogeochem. Cycles.* https://doi.org/10.1029/2010GB003793 (2010).

17. Cabaço, S. & Santos, R. Human-induced changes of the seagrass *Cymodocea nodosa* in Ria Formosa lagoon (Southern Portugal) after a decade. *Cah. Biol. Mar.* **55**, 101–108 (2014).
18. Marbà, N., Krause-Jensen, D., Masqué, P. & Duarte, C. M. Expanding Greenland seagrass meadows contribute new sediment carbon sinks. *Sci. Rep.* **8**, 1–8 (2018).
19. Bañolas, G., Fernández, S., Espino, F., Haroun, R. & Tuya, F. Evaluation of carbon sinks by the seagrass *Cymodocea nodosa* at an oceanic island: Spatial variation and economic valuation. *Ocean Coast. Manag.* **187**, 105112 (2020).
20. Duarte, C. M. & Krause-Jensen, D. Export from seagrass meadows contributes to marine carbon sequestration. *Front. Mar. Sci.* **4**, 13 (2017).
21. Duarte, C. M., Middelburg, J. J. & Caraco, N. Major role of marine vegetation on the oceanic carbon cycle. *Biogeosci.* **2**, 1–8 (2005).
22. Kennedy, H. *et al.* Seagrass sediments as a global carbon sink: Isotopic constraints. *Glob. Biogeochem. Cycles* https://doi.org/10.1029/2010GB003848 (2010).
23. Orth, R. J. *et al.* A global crisis for seagrass ecosystems. *Bioscience* **56**, 987–996 (2006).
24. Waycott, M. *et al.* Accelerating loss of seagrasses across the globe threatens coastal ecosystems. *Proc. Natl. Acad. Sci.* **106**, 12377–12381 (2009).
25. Arias-Ortiz, A. *et al.* A marine heatwave drives massive losses from the world's largest seagrass carbon stocks. *Nat. Clim. Change* **8**, 338 (2018).
26. Collier, C. J. *et al.* Optimum temperatures for net primary productivity of three tropical seagrass species. *Front. Plant Sci.* **8**, 1446 (2017).
27. George, R., Gullström, M., Mangora, M. M., Mtolera, M. S. & Björk, M. High midday temperature stress has stronger effects on biomass than on photosynthesis: a mesocosm experiment on four tropical seagrass species. *Ecol. Evol.* **8**, 4508–4517 (2018).
28. Savva, I., Bennett, S., Roca, G., Jordà, G. & Marbà, N. Thermal tolerance of Mediterranean marine macrophytes: Vulnerability to global warming. *Ecol. Evol.* **8**, 12032–12043 (2018).
29. Massa, S. I., Arnaud-Haond, S., Pearson, G. A. & Serrão, E. A. Temperature tolerance and survival of intertidal populations of the seagrass *Zostera noltii* (Hornemann) in Southern Europe (Ria Formosa, Portugal). *Hydrobiologia* **619**, 195–201 (2009).
30. Bergmann, N. *et al.* Population-specificity of heat stress gene induction in northern and southern eelgrass *Zostera marina* populations under simulated global warming. *Mol. Ecol.* **19**, 2870–2883 (2010).
31. Franssen, S. U. *et al.* Genome-wide transcriptomic responses of the seagrasses *Zostera marina* and *Nanozostera noltii* under a simulated heatwave confirm functional types. *Mar. Genomics* **15**, 65–73 (2014).
32. Qin, L. Z. *et al.* Influence of regional water temperature variability on the flowering phenology and sexual reproduction of the seagrass *Zostera marina* in Korean coastal waters. *Estuaries Coasts* **43**, 449–462 (2020).
33. Gao, Y. *et al.* Photosynthetic and metabolic responses of eelgrass *Zostera marina L.* to short-term high-temperature exposure. *J. Oceanol. Limnol.* **37**, 199–209 (2019).
34. Marín-Guirao, L. *et al.* Carbon economy of Mediterranean seagrasses in response to thermal stress. *Mar. Pollut. Bull.* **135**, 617–629 (2018).
35. Costa, M. M., Silva, J., Barrote, I. & Santos, R. Heatwave effects on the photosynthesis and antioxidant activity of the seagrass *Cymodocea nodosa* under contrasting light regimes. *Oceans* **2**, 448–460 (2021).
36. de los Santos, C. *et al.* Recent trend reversal for declining European seagrass meadows. *Nat. Commun.* **10,** 3356 (2019).
37. Cunha, A. H., Assis, J. F. & Serrão, E. A. Reprint of "Seagrasses in Portugal: A most endangered marine habitat". *Aquat. Bot.* **115**, 3–13 (2014).
38. Olsen, Y. S., Sánchez-Camacho, M., Marbà, N. & Duarte, C. M. Mediterranean seagrass growth and demography responses to experimental warming. *Estuaries Coasts* **35**, 1205–1213 (2012).
39. Marín-Guirao, L., Ruiz, J. M., Dattolo, E., Garcia-Munoz, R. & Procaccini, G. Physiological and molecular evidence of differential short-term heat tolerance in Mediterranean seagrasses. *Sci. Rep.* **6**, 1–13 (2016).
40. Lüning, K. *Seaweeds. Their Environment, Biogeography, and Ecophysiology* (Wiley-Interscience, New York, 1990).
41. Lee, K. S., Park, S. R. & Kim, Y. K. Effects of irradiance, temperature, and nutrients on growth dynamics of seagrasses: a review. *J. Exp. Mar. Biol. Ecol.* **350**, 144–175 (2007).
42. Franssen, S. U. *et al.* Transcriptomic resilience to global warming in the seagrass *Zostera marina*, a marine foundation species. *Proc. Natl. Acad. Sci.* **108**, 19276–19281 (2011).
43. Winters, G., Nelle, P., Fricke, B., Rauch, G. & Reusch, T. B. H. Effects of a simulated heat wave on photophysiology and gene expression of high- and low-latitude populations of *Zostera marina*. *Mar. Ecol. Prog. Ser.* **435**, 83–95 (2011).
44. Maxwell, K. & Johnson, G. N. Chlorophyll fluorescence—A practical guide. *J. Exp. Bot.* **51**, 659–668 (2000).
45. Schubert, N. *et al.* Photoacclimation strategies in northeastern Atlantic seagrasses: Integrating responses across plant organizational levels. *Sci. Rep.* **8**, 1–14 (2018).
46. Miyake, C., Yonekura, K., Kobayashi, Y. & Yokota, A. Cyclic electron flow within PSII functions in intact chloroplasts from spinach leaves. *Plant Cell Physiol.* **43**, 951–957 (2002).
47. Rasmusson, L. M., Gullström, M., Gunnarsson, P. C. B., George, R. & Björk, M. Estimation of a whole plant Q10 to assess seagrass productivity during temperature shifts. *Sci. Rep.* **9**, 1–9 (2019).
48. Buapet, P. & Björk, M. The role of O_2 as an electron acceptor alternative to CO_2 in photosynthesis of the common marine angiosperm *Zostera marina* L. *Photosynth. Res.* **129**, 59–69 (2016).
49. Mehler, A. H. Studies on reactions of illuminated chloroplasts. II Stimulation and inhibition of the reaction with molecular oxygen. *Arch. Biochem. Biophys.* **34**, 339–51 (1951).
50. Apel, K. & Hirt, H. Reactive oxygen species: metabolism, oxidative stress, and signal transduction. *Annu. Rev. Plant Biol.* **55**, 373–399 (2004).
51. Chalanika De Silva, H. C. & Asaeda, T. Effects of heat stress on growth, photosynthetic pigments, oxidative damage and competitive capacity of three submerged macrophytes. *J. Plant Interact.* **12**, 228–236 (2017).
52. Beer, S., Björk, M., Gademann, R. & Ralph, P. Measurements of photosynthetic rates in seagrasses. In *Global Seagrass Research Methods* pp. 183–198 (Elsevier Science, 2001).
53. Brodersen, K. E., Kühl, M., Nielsen, D. A., Pedersen, O. & Larkum, A. W. Rhizome, root/sediment interactions, aerenchyma and internal pressure changes in seagrasses. In *Seagrasses of Australia* pp. 393–418; https://doi.org/10.1007/978-3-319-71354-0_13 (Springer, Cham, 2018).
54. Purnama, P. R., Purnama, E. R., Manuhara, Y. S. W., Hariyanto, S. & Purnobasuki, H. Effect of high temperature stress on changes in morphology, anatomy and chlorophyll content in tropical seagrass *Thalassia hemprichii*. *AACL Bioflux* **11**, 1825–1833 (2018).
55. Rosalina, D., Herawati, E. Y., Musa, M., Sofarini, D. & Risjani, Y. Anatomical changes in the roots, rhizomes and leaves of seagrass (*Cymodocea serrulata*) in response to lead. Biodiversitas **20,** 2583–2588; https://doi.org/10.13057/biodiv/d200921 (2019).
56. Beca-Carretero, P., Olesen, B., Marbà, N. & Krause-Jensen, D. Response to experimental warming in northern eelgrass populations: comparison across a range of temperature adaptations. *Mar. Ecol. Progr. Ser.* **589,** 59–72; https://doi.org/10.3354/meps12439 (2018).
57. Beca-Carretero, P., Guihéneuf, F., Krause-Jensen, D. & Stengel, D. B. Seagrass fatty acid profiles as a sensitive indicator of climate settings across seasons and latitudes. *Mar. Env. Res.* **161,** 105075; https://doi.org/10.1016/j.marenvres.2020.105075 (2020).
58. Pérez, M. & Romero, J. Photosynthetic response to light and temperature of the seagrass *Cymodocea nodosa* and the prediction of its seasonality. *Aquat. Bot.* **43,** 51–62; https://doi.org/10.1016/0304-3770(92)90013-9 (1992).

59. Saha, M. *et al*. Response of foundation macrophytes to near-natural simulated marine heatwaves. *Global Change Biol.* **26,** 417–430; https://doi.org/10.1111/gcb.14801 (2020).
60. Tutar, O., Marín-Guirao, L., Ruiz, J. M. & Procaccini, G. Antioxidant response to heat stress in seagrasses. A gene expression study. *Mar. Environ. Res.* **132,** 94–102; https://doi.org/10.1016/j.marenvres.2017.10.011 (2017).
61. Moreno-Marín, F., Brun, F. G. & Pedersen, M. F. Additive response to multiple environmental stressors in the seagrass *Zostera marina* L. *Limnol. Oceanogr.* **63,** 1528–1544; https://doi.org/10.1002/lno.10789 (2018).
62. Kim, M. *et al*. Influence of water temperature anomalies on the growth of *Zostera marina* plants held under high and low irradiance levels. *Estuaries Coasts* **43,** 463–476; https://doi.org/10.1007/s12237-019-00578-2 (2020).
63. Egea, L. G., Jiménez-Ramos, R., Vergara, J. J., Hernández, I. & Brun, F. G. Interactive effect of temperature, acidification and ammonium enrichment on the seagrass *Cymodocea nodosa*. *Mar. Pollut. Bull.* **134,** 14–26; https://doi.org/10.1016/j.marpolbul.2018.02.029 (2018).
64. Newton, A. & Mudge, S. M. Temperature and salinity regimes in a shallow, mesotidal lagoon, the Ria Formosa, Portugal. *Estuarine Coastal Shelf Sci.* **57,** 73–85; https://doi.org/10.1016/S0272-7714(02)00332-3 (2003).
65. Instituto Hidrográfico. *Marés 81/82 Ria de Faro. Estudo das marés de oito estacões da Ria de Faro* pp. 13 (Lisbon: Instituto Hidrográfico, 1986).
66. Andrade, J. P. *Aspectos Geomorfológicos, Ecológicos e Socioeconómicos da Ria Formosa* pp. 91 (Faro: Universidade do Algarve, 1985).
67. Hobday, A.J. *et al*. A hierarchical approach to defining marine heatwaves. *Prog. Oceanogr.* **141,** 227–238; https://doi.org/10.1016/j.pocean.2015.12.014 (2016).
68. Hobday, A. J. *et al*. Categorizing and naming marine heatwaves. *Oceanogr.* **31,** 162–173; https://doi.org/10.5670/oceanog.2018.205 (2018).
69. Cunha, A. H., Paulo, D. S., Sousa, I. & Serrão, E. The rediscovery of *Caulerpa prolifera* in Ria Formosa, Portugal, 60 years after the previous record. *Cah. Biol. Mar.* **54**, 359–364 (2013).
70. Huang, B. *et al*. Improvements of the daily optimum interpolation sea surface temperature (DOISST) Version 2.1. *J. Clim.* **34**, 2923–2939 (2020).
71. Reynolds, R. W. *et al*. Daily high-resolution-blended analyses for sea surface temperature. *J. Clim.* **20**, 5473–5496 (2007).
72. Banzon, V., Smith, T. M., Chin, T. M., Liu, C. & Hankins, W. A long-term record of blended satellite and in situ sea-surface temperature for climate monitoring, modelling and environmental studies. *Earth Syst. Sci. Data* **8**, 165–176 (2016).
73. Schlegel, R. W. Marine Heatwave Tracker. http://www.marineheatwaves.org/tracker; 10.5281/zenodo.3787872 (2020).
74. Field, C. B., Barros, V., Stocker, T. F. & Dahe, Q. (Eds.). Managing the risks of extreme events and disasters to advance climate change adaptation: special report of the intergovernmental panel on climate change (IPCC) (Cambridge University Press, 2012).
75. Silva, J., Barrote, I., Costa, M. M., Albano, S. & Santos, R. Physiological responses of *Zostera marina* and *Cymodocea nodosa* to light-limitation stress. *PLoS One* **8**, e81058 (2013).
76. Silva, J. & Santos, R. Can chlorophyll fluorescence be used to estimate photosynthetic production in the seagrass *Zostera noltii*?. *J. Exp. Mar. Biol. Ecol.* **307**, 207–216 (2004).
77. Jassby, A. D. & Platt, T. Mathematical formulation of the relationship between photosynthesis and light for phytoplankton. *Limnol. Oceanogr.* **21**, 540–547 (1976).
78. Henley, W. J. Measurement and interpretation of photosynthetic light-response curves in algae in the context of photoinhibition and diel changes. *J. Phycol.* **29**, 729–739 (1993).
79. Genty, B., Briantais, J. M. & Baker, N. R. The relationship between the quantum yield of photosynthetic electron transport and quenching of chlorophyll fluorescence. *Biochim. Biophys. Acta* **990**, 87–92 (1989).
80. Folin, O. & Ciocalteu, V. On tyrosine and tryptophane determinations in proteins. *J. Biol. Chem.* **73**, 627–650 (1927).
81. Booker, F. L. & Miller, J. E. Phenylpropanoid metabolism and phenolic composition of soybean [Glycine max (L) Merr] leaves following exposure to ozone. *J. Exp. Bot.* **49**, 1191–1202 (1998).
82. Re, R. *et al*. Antioxidant activity applying an improved ABTS radical cation decolorization assay. *Free Radical Biol. Med.* **26**, 1231–1237 (1999).
83. Gillespie, K. M., Chae, J. M. & Ainsworth, E. A. Rapid measurement of total antioxidant capacity in plants. *Nat. Protoc.* **2**, 867–870 (2007).
84. Huang, D., Ou, B., Hampsch-Woodill, M., Flanagan, J. A. & Prior, R. L. High-Throughput Assay of Oxygen Radical Absorbance Capacity (ORAC) Using a Multichannel Liquid Handling System Coupled with a Microplate Fluorescence Reader in 96-Well Format. *J. Agric. Food Chem.* **50**, 4437–4444 (2002).
85. Hodges, D. M., DeLong, J. M., Forney, C. F. & Prange, R. K. Improving the thiobarbituric acid-reactive-substances assay for estimating lipid peroxidation in plant tissues containing anthocyanin and other interfering compounds. *Planta* **207**, 604–611 (1999).
86. Rasband, W.S. ImageJ, U. S. National Institutes of Health, Bethesda, Maryland, USA, 1997–2018. https://imagej.nih.gov/ij/ (1997).
87. R Core Team. R: A language and environment for statistical computing. R Foundation for Statistical Computing, Vienna, Austria. http://www.R-project.org/ (2014).
88. Devore, J. & Farnum, N. *Applied Statistics for Engineers and Scientists* (ed. Brooks/Cole) pp. 656 (Pacific Grove, CA, USA, 1999).

Acknowledgements

The authors wish to thank Diogo Paulo from CCMAR's Scientific Diving Centre for the support in plant collection, João Reis and Miguel Patusco from CCMAR's Experimental Marine Station at Ramalhete for their extensive technical support with the mesocosm system, and Manuela David, curator of ALGU Herbarium, for supervising tasks involving the identification, preparation and deposit of the voucher specimens. This work was financed by Portuguese national funds from FCT—Fundação para a Ciência e a Tecnologia through project UIDB/04326/2021, and from the operational programmes CRESC Algarve 2020 and COMPETE 2020 through project EMBRC.PT ALG-01-0145-FEDER-022121.

Author contributions

J.S. and I.B. conceived the study and designed the experimental approach; A.D. and I.B. performed the laboratory analyses; A.D. and J.S. performed the P-I curves and the CFI analysis; A.D. analysed the data and performed the statistical analyses; A.D. led the writing of the manuscript. All authors reviewed the manuscript.

Competing interests

The authors declare no competing interests.

Additional information

Supplementary Information The online version contains supplementary material available at https://doi.org/10.1038/s41598-022-12102-x.

Correspondence and requests for materials should be addressed to J.S.